Engineering Applications of Artificial Intelligence 129 (2024) 107380

Contents lists available at ScienceDirect

Engineering Applications of Artificial Intelligence

journal homepage: www.elsevier.com/locate/engappai

Refined self-attention mechanism based real-time structural response prediction method under seismic action

Shiqiao Meng , Ying Zhou *, Zhiyuan Gao

State Key Laboratory of Disaster Reduction in Civil Engineering, Tongji University, Shanghai, China

ARTICLE INFO

Keywords:
Structural seismic response prediction
SeisFormer
Self-attention mechanism
Earthquake engineering
Data-driven machine learning

ABSTRACT

Accurate prediction of structural response under earthquake is of great significance for structural damage and performance evaluation. In order to improve the efficiency of structure time history response prediction, this paper proposes a novel SeisFormer model based on the self-attention mechanism and deep learning technology. Through autoregressive prediction, the SeisFormer can achieve real-time prediction of the response time histories of a large number of nodes in the structure under seismic action and can effectively solve the problem of data scarcity. Four case studies are performed to verify the accuracy and efficiency of the proposed methodology, including validation on datasets obtained from elastoplastic seismic analysis of a single-story structure, a three-story structure, and an eleven-story structure, and measured data of a shaking table test model. In addition, this paper further studies the prediction accuracy of the SeisFormer through ablation experiments and comparative experiments. The experimental results show that the SeisFormer can accurately predict the acceleration, velocity, and displacement time histories of numerous nodes in the structure. The prediction accuracy outperforms the LSTM model, and the prediction speed is 193–109,824 times faster than finite element method. Furthermore, with data augmentation through autoregressive prediction, the SeisFormer model can achieve efficient and accurate predictions when training data is exceptionally scarce, enabling engineering applications.

1. Introduction

Earthquake hazards are among the most catastrophic hazards globally, causing major economic effects and moralities (Zhou et al., 2017). When a structure is subjected to an earthquake, the structure will deform due to external forces, which may lead to the destruction or even collapse of the entire structure. However, once the seismic response can be rapidly predicted, the structure can be better protected from earthquakes by applying the predicted time histories to seismic vulnerability assessment (Morfidis and Kostinakis, 2018), structural health monitoring (Oh et al., 2020), and seismic design improvements. In addition, guiding strategies for post-disaster rescue or recovery can also be provided. Therefore, the prediction of seismic dynamic response, especially the prediction of time history, is critical in earthquake engineering.

Nonlinear dynamic analysis is widely used in buildings of considerable height and fortification strength or fairly irregular buildings to obtain structural response time histories. It achieves time history forecasting by progressively considering the nonlinear properties and geometric nonlinearities of materials in a specified time series. Numerical implementations of time history analysis have been studied for decades (Bretas et al., 2016; Nie et al., 2022). Among them, the most prevalent numerical method is the Finite Element Method (FEM) (Mohan and Prabha, 2011; Wilkinson and Hiley, 2006; Asgarieh et al., 2014). However, the applicability of these physics-based numerical methods for real-time damage prediction is limited due to the uncertainty of real structures and the enormous calculation. There must be a trade-off between accuracy and computational speed, so real-time forecasting is still a long way off.

With the development of computing capability and the theory of deep learning (DL) in the past decades (Ketkar and Santana, 2017), more and more researchers resort to artificial intelligence to solve civil engineering problems that are physically and computationally prohibitively complex when applying traditional mechanical methods (Hou and Liu, 2022; Wang and Adeli, 2015; Nikolopoulos et al., 2022; Naser, 2019). According to the universal approximation theorem, an artificial neural network (ANN) can provide approximate end-to-end solutions by establishing a mapping relationship model in many earthquake engineering situations (Zhang et al., 2020a). An extensive range of research

* Corresponding author.
E-mail address: yingzhou@tongji.edu.cn (Y. Zhou).

https://doi.org/10.1016/j.engappai.2023.107380
Received 23 July 2022; Received in revised form 9 February 2023; Accepted 25 October 2023
Available online 29 November 2023

has proven this method's feasibility and promising future (Azimi and Pekcan, 2020; Liang, 2019). Some researchers utilized ANN to predict the maximum interstorey drift ratio (MIDR) to estimate the structural damage under seismic action. Nevertheless, MIDR is a more macroscopic damage index, which is easier to acquire than the response time history and has limited utility (Morfidis and Kostinakis, 2018; Oh et al., 2020).

In recent years, there have been many studies on the time history prediction of structural response based on deep learning. Jiang and Adeli (2005) implemented a three-layer neural network (wavelet neural network (WNN) (Jiang and Adeli, 2005)) to predict the acceleration time history of the second floor of a five-story steel frame by using the acceleration time sequence of the first, second and third floors (Adeli and Jiang, 2006). Wu and Jahanshahi (2019) adopt a deep convolutional neural network (CNN) for response time history estimation and validate it with a three-story steel frame. However, due to the limitation of the neural network structure, the information on the time dimension is lost. Perez-Ramirez et al. (2019) overcame the drawback mentioned above by surrogating those models with recurrent neural network (RNN) and successfully made time history prediction in a sequence-to-sequence and autoregressive way. Some researchers have used LSTM networks to achieve structural response prediction under seismic action at individual locations through various methods, such as adding physical information (Zhang et al., 2019, 2020a,b; Gao and Zhang, 2020; Yu et al., 2020; Peng et al., 2021; Xu et al., 2022). With the rapid development of the self-attention mechanism in natural language processing (Vaswani et al., 2017), some researchers have added the self-attention mechanism to the structural response prediction model, thus realizing the prediction of the displacement time history (Li et al., 2021a,b).

Previous studies have proposed solutions for single-node seismic response prediction. However, these proposed methods also suffer from limitations. Firstly, only predicting the structural response of floors or only a small number of nodes of the whole structure is too coarse for practical application to enable refined seismic hazard assessment. Besides, models such as LSTM suffer from cumulative and significant errors in making predictions. The vanishing gradient problem will likely occur when the input time series is quite long, making the model ineffective in predicting long series. Finally, due to the extremely high time and computational resources required for finite element elastoplastic calculations, it is challenging to obtain response time history datasets of structures under seismic actions in engineering applications, resulting in an extreme shortage of training samples. The advantages of deep learning cannot be effectively utilized.

In order to overcome the shortcomings of previous prediction methods, this study proposes a novel SeisFormer model based on the self-attention mechanism, which predicts the response time histories of a large number of nodes in the structure through autoregression, extending the research in this field to the engineering application level. Thus, a real-time intelligent seismic effect evaluation system is established. Compared with existing research, the innovations and findings of this study are as follows:

1. The proposed SeisFormer model based on the multi-head self-attention mechanism can give full play to the advantages of rapid prediction methods in earthquake engineering compared with traditional methods. First, the simultaneous prediction of multiple time-step responses significantly improves prediction accuracy while enhancing prediction speed. Furthermore, refined real-time structural damage assessment is possible by simultaneously predicting a large number of nodes in a building. Finally, the gradient vanishing problem of the model during model training can be effectively solved.
2. Through the elastoplastic calculation of the refined finite element model, the structural response time history of all nodes on the structure can be obtained in large quantities as the training data of the model. Furthermore, since subsequences of seismic wave records are inputed through an autoregressive strategy, the demand for the number of seismic waves in the dataset is significantly reduced, thus solving the problem of data scarcity and significantly improving the robustness of the model.

The rest of the paper is organized as follows: Section 2 introduces the mechanism of structural seismic response prediction through autoregression, the pipeline of our prediction method, and the architecture of the proposed SeisFormer. Section 3 presents four case studies to validate our methodology through experiments. In addition, the hyperparameters in the SeisFormer are investigated through ablation studies, and the prediction accuracy of the SeisFormer and the LSTM is also compared through comparative experiments. Section 4 draws a conclusion of this study.

2. Structural response prediction method based on SeisFormer

2.1. Structural dynamic response under seismic action

The dynamic motion equation of a structure under seismic action can be expressed as follows:

$$M\ddot{x}(t) + C\dot{x}(t) + Kx(t) = M\Gamma\ddot{x_g}(t) \tag{1}$$

where M is the mass matrix, C is the damping matrix, K is the stiffness matrix; Γ is the force distribution vector; $\ddot{x}$, $\dot{x}$, and x represent the structure's corresponding acceleration, velocity, and displacement, respectively; $\ddot{x_g}$ is the ground acceleration.

The second-order problem, governed by the differential equation of motion expressed in matrix form, can be converted into two first-order problems with state-space models. The state vector $s(t)$ can be expressed as:

$$s(t) = \begin{Bmatrix} \dot{x}(t) \\ x(t) \end{Bmatrix} \tag{2}$$

Therefore, Eq. (1) can be rewritten as:

$$\dot{s}(t) = A_c s(t) + B_c \ddot{x}_g(t) \tag{3}$$

$$A_c = \begin{bmatrix} -M^{-1}C & -M^{-1}K \\ I & 0 \end{bmatrix} \tag{4}$$

$$B_c = \begin{bmatrix} M^{-1}\Gamma \\ 0 \end{bmatrix} \tag{5}$$

The observation equation for the structure can be expressed as:

$$x_l(t) = C_a\ddot{x}(t) + C_v\dot{x}(t) + C_d x(t) \tag{6}$$

where x_l is the vector of the measured outputs, which can represent measurements of the structural response taken at l locations; C_a, C_v, and C_d are the output location matrices for acceleration, velocity, and displacement, respectively. Substituting Eqs. (1) and (2) into Eq. (6) yields the following equation:

$$x_l(t) = C_c x(t) + D_c \ddot{x}_g(t) \tag{7}$$

$$C_c = \begin{bmatrix} C_v - C_a M^{-1}C & C_d - C_a M^{-1}K \end{bmatrix} \tag{8}$$

$$D_c = C_a M^{-1}\Gamma \tag{9}$$

By introducing the zero-order hold assumption, the continuous-time equation can be discretized and solved at all discrete instants so that a continuous-time state-space model can be converted into a discrete-time state-space model (Rainieri and Fabbrocino, 2014):

$$\begin{cases} s_{k+1} = A_s s_k + B_s \ddot{x}_{g,k} \\ x_k = C_s s_k + D_s \ddot{x}_{g,k} \end{cases} \tag{10}$$

$$\begin{cases} A_s = e^{A_c \Delta t} \\ B_s = (A_s - I)A_c^{-1}B_c \\ C_s = C_c \\ D_s = D_c \end{cases} \tag{11}$$

where Δt is the sampling period; A_s is the discrete state matrix, B_s is the discrete input matrix, C_s is the discrete output matrix and D_s is the direct transmission matrix.

Since the state vector s_0 of the building is equal to 0 at the initial moment of structural response analysis under seismic action, x_k can be expressed as:

$$x_k = C_s A_s^{k-1} B_s \ddot{x}_{g,1} + C_s A_s^{k-2} B_s \ddot{x}_{g,2} + \ldots + C_s A_s B_s \ddot{x}_{g,k-1} + C_s B_s \ddot{x}_{g,k} + D_s \ddot{x}_{g,k} \tag{12}$$

If the matrix $(C_s B_s + D_s)$ is invertible, after expressing x_{k-1} with Eq. (12), then $\ddot{x}_{g,k-1}$ can be expressed as:

$$\ddot{x}_{g,k-1} = (C_s B_s + D_s)^{-1} \left(x_{k-1} - C_s A_s^{k-2} B_s \ddot{x}_{g,1} - \ldots - C_s A_s B_s \ddot{x}_{g,k-2} \right) \tag{13}$$

Substituting $\ddot{x}_{g,k-1}$, $\ddot{x}_{g,k-2}$, …, $\ddot{x}_{g,1}$ into Eq. (12) in turn shows that x_k can be affected by x_{k-1}, x_{k-2}, …, x_1 and $\ddot{x}_{g,k}$. Therefore, combined with Eq. (12), x_k can be expressed as:

$$x_k = f\left(x_{k-1}, x_{k-2}, \ldots, x_1, \ddot{x}_{g,k}, \ddot{x}_{g,k-1}, \ldots, \ddot{x}_{g,1} \right) \tag{14}$$

where f represents a multi-variable linear function model. Since the damping matrix C and stiffness matrix K of the structure change with time in the elastoplastic seismic analysis, the function f in Eq. (14) is a nonlinear function in that case. Through the initial state relaxation (Peng et al., 2021), x_k can be expressed by:

$$x_k = g\left(x_{k-N}, x_{k-N+1}, \ldots, x_{k-2}, x_{k-1}, \ddot{x}_{g,k-N}, \ddot{x}_{g,k-N+1}, \ldots, \ddot{x}_{g,k-1}, \ddot{x}_{g,k} \right) \tag{15}$$

where g represents a multi-variable nonlinear function model.

This paper establishes a nonlinear function through a deep learning-based model called SeisFormer. It uses the ground motion information and the historical response of the structure to predict the future response of the structure efficiently.

2.2. The overall process of structural response prediction under seismic action

In order to conduct a more detailed, comprehensive, and refined response time history analysis of the structure under seismic action, it is necessary to obtain the refined finite element model of the structure to generate the dataset. The refined finite element model refers to the finite element model with detailed finite element mesh division. In addition, the structural components of the building are modeled in detail in the refined finite element model, so the results of the finite element calculation are very accurate.

The overall process proposed in this paper is as follows: First, a refined finite element model of the structure needs to be established, and some measured seismic data in the seismic database is selected as the input of the time history analysis. The amplitude of the seismic wave needs to be modulated according to the seismic protection intensity. After that, the time history data of each node in the structure, including acceleration, velocity, and displacement, are obtained through elastoplastic finite element calculation. Select the time histories of the nodes, and make it the input data and ground-truth of the SeisFormer through data preprocessing. Finally, a trained model can be obtained by using these data to train the SeisFormer and using backpropagation to iteratively optimize the weights in the neural network during the training process. When a new earthquake occurs, the trained model can be used to forecast the response time histories of some or all nodes of the structure in real-time accurately. A schematic diagram of the above overall process is shown in Fig. 1.

Due to the high time-consuming calculation of elastoplastic finite elements for structures, it is difficult to obtain a large amount of data for the deep-learning model. Therefore, to fully use the limited dataset, the proposed SeisFormer model uses an autoregressive way to make predictions.

Since the model training is carried out through autoregressive iterative prediction, a seismic wave can be divided into thousands of training samples through overlapping partition, so the problem of lack of data can be solved to a large extent. The method of overlapping partition will be introduced in detail in Section 3.1.3. It should be noted that in the training phase of the model, the data set is augmented through the overlapping partition. However, in the model testing stage, the structural response is the unknown data that needs to be predicted, and the seismic wave is the known data. Therefore, during the testing phase, the model inference must be performed many times to generate predicted structural responses in chronological order in an autoregressive manner. Among them, it is necessary to use the structural response obtained from the previous model predictions as the input of the following model inference. In addition, through those mentioned above autoregressive technical routes, the model only forecasts the short-term structural response, which reduces the difficulty of long-term prediction for the model, thereby improving the prediction accuracy.

The input of the SeisFormer model is the historical response time histories of all nodes and ground motion in multiple time steps before the current moment and the ground motion of multiple time steps after the current moment. The output result is the predicted response time histories of all nodes of multiple time steps after the current moment.

When predicting the structural response of the entire seismic wave by autoregression, the model iteratively uses the predicted structural response time histories at the previous moment and the seismic waves until all the ground motion data are processed. The input ground motion information and the node's response time histories information need to be the same type of response. A schematic diagram of the above process is shown in Fig. 2.

It is worth mentioning that compared to RNN-based networks such as LSTM networks. One advantage of SeisFormer proposed in this paper is that it can reduce cumulative error to a certain extent. The cumulative error mentioned here mainly refers to the stepwise forecasting in each divided series in autoregressive forecasting. When the LSTM network performs time series prediction, due to the network structure, it needs to output the prediction results step by step, which uses the prediction results of the previous time step as the input of the next time step. The proposed SeisFormer prediction method in this paper is to directly output the prediction results of the following multiple time steps, and there is no iteration by time step. Therefore, the proposed SeisFormer can reduce the cumulative error compared to LSTM.

2.3. Structure of the SeisFormer model

The SeisFormer model proposed in this paper consists of a preprocessing module, stacked SeisBlocks, and a fully connected layer. Through the SeisFormer, structural response time histories can be predicted for multiple time steps in one forward propagation calculation, which can achieve more efficient and accurate prediction result compared with other models such as LSTM and TransFormer models. The overall structure of the SeisFormer is shown in Fig. 3.

2.3.1. The preprocessing module

The function of the preprocessing module is to extract features from the seismic time history data and ground motion data. This module's core idea is to fuse multiple nodes' information through the convolutional layer and embed it into higher-dimensional features.

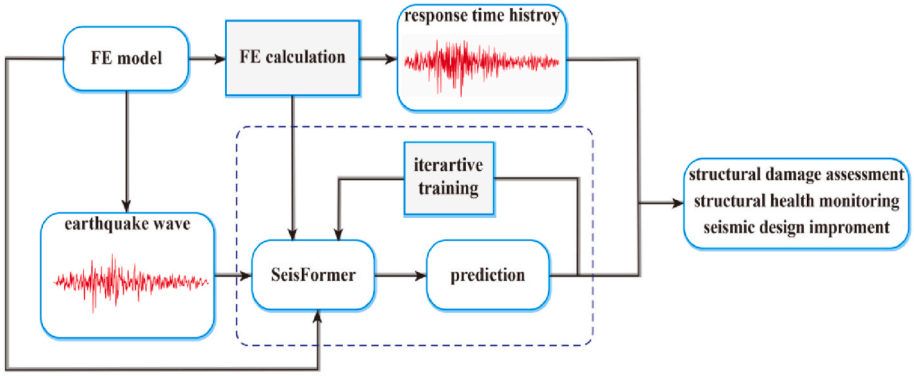

Fig. 1. Overall flow chart of real-time prediction method of structural response under seismic action.

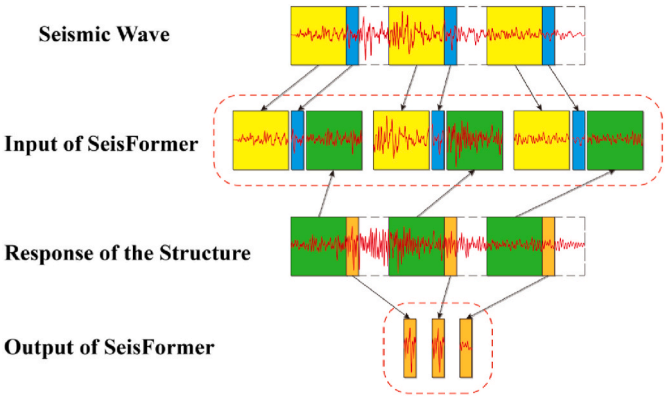

Fig. 2. Schematic diagram of input and output data of the SeisFormer.

The data processed by the preprocessing module are the node response time history data of the last i time steps and the ground motion data of the last i time steps and the next j time steps. Two types of data are processed and added by using a one-dimensional convolutional layer with a kernel size of 1×1, where the number of input channels of the convolutional layer is 1, and the number of output channels is the dimension of the input features of the SeisBlock, which is 512 in this paper. It should be noted that when dealing with a single node, it is necessary to align the structural response with the ground motion in the time dimension. Since the structural response of the next j time steps is unknown, the structural response of the next j time steps needs to be zero-filled. The data of all nodes need to be added after the above processing to realize feature fusion. In order to make the model capable of distinguishing the time relationship of the input data, positional embedding needs to be added to the input. Through positional embedding, the absolute position sequence of the input data can be encoded into the feature of the input model, which is only related to the input data's absolute position rather than the data's specific value. The positional embedding used in this article is the same as in TransFormer (Vaswani et al., 2017), which is encoded by the sine function.

The expression of the preprocessing module is shown in Eq. (16):

$$F = \sum_{k=1}^{N} \left(Conv\left(E_{t-i,k}, E_{t-i+1,k}, \ldots, E_{t,k}, E_{t+1,k}, \ldots, E_{t+j,k}\right) + Conv\left(R_{t-i,k}, R_{t-i+1,k}, \ldots, R_{t-1,k}\right) \right) + PE \tag{16}$$

where $Conv$ represents convolutional layer; PE represents positional embedding; t is the current time step; E is the ground motion data; R is the response time history data, N indicates the total number of all nodes, and F is the output result of the preprocessing module. The data of each node is processed by Eq. (16) to obtain a two-dimensional tensor, which can be input into SeisBlock for subsequent processing.

2.3.2. The SeisBlock module

The SeisBlock module proposed in this paper consists of two multi-head linear self-attention modules, multiple dropout layers (Srivastava et al., 2014), LayerNorm layers, and a Feed-Forward module. The schematic diagram of the overall structure of SeisBlock is shown in Fig. 4 (b).

The input of the SeisBlock module is the output feature of the preprocessing module or the output result of the SeisBlock module in the previous layer. The input feature is the multi-head linear self-attention module's key, value, and query features. And then, the dropout layer is used to reduce the effect of model overfitting, and the LayerNorm layer is used to normalize the features. The reason for normalizing the features is to stabilize the parameters of this layer, avoid gradient disappearance or gradient explosion, and facilitate subsequent neural network learning. Using LayerNorm instead of other normalization methods can preserve the size relationship between different features within a sample. The expression of the LayerNorm layer is shown in Eq. (17).

$$y = \frac{x - E(x)}{\sqrt{Var(x) + \epsilon}} * \gamma + \beta \tag{17}$$

where y represents the output of the LayerNorm layer; x is the input of the LayerNorm layer; $E(x)$ means the mean of x over each sample; $\mathrm{Var}(x)$ is the variance of x over each sample; ϵ is a small positive number; γ and β are the weights and biases of the LayerNorm layer, respectively, which can be dynamically optimized during model training. In this way, the gradient explosion phenomenon of the model during the training process can be prevented.

CNN or RNN can only characterize the short-distance correlation of the input information, and even the LSTM that introduces the gating mechanism can only characterize the specific long-distance correlation. The self-attention mechanism used in the TransFormer (Vaswani et al., 2017) model can dynamically generate the weights of different connections so that the weights are related to the importance of the data itself. In addition, the RNN-based model is difficult to calculate in parallel and can only output results step by step, which the self-attention mechanism model can solve. The self-attention mechanism mainly performs linear transformation on the query, key, and value vectors and combines the above vectors through scaled dot-product attention, which significantly improves the fitting ability of the model. The role of the query vector is to query the relationship between itself and other inputs. The key vector is provided to other vectors to find the relationship with itself. And the role of the value vector is to represent the feature of the input and linearly combine with the weight generated by the query vector and the key vector. The query, key, and value vector in the self-attention mechanism come from the same sequence. Using eight linear self-attention modules to process features and information in parallel can achieve attention to different types of information. Therefore, the input tensor is divided into 8 tensors with a channel size of 64

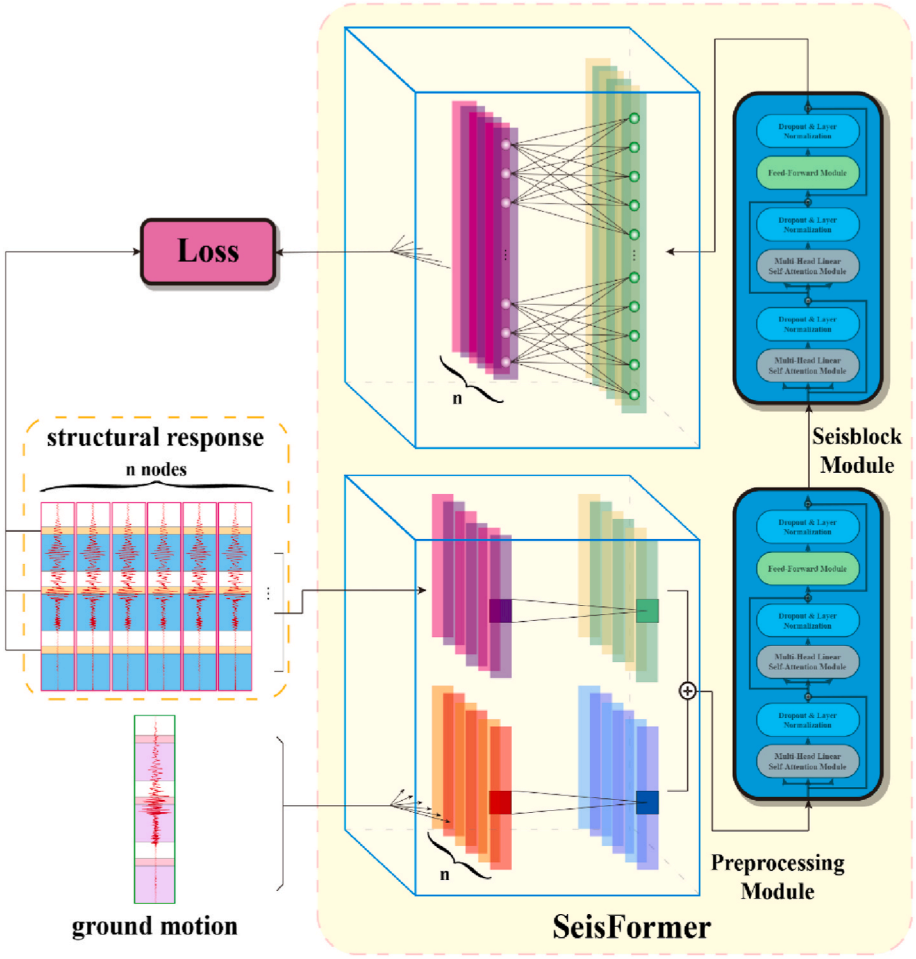

Fig. 3. The overall structure of the SeisFormer.

from the channel dimension, and the self-attention mechanism is used for processing, respectively.

Fig. 4(a) shows the schematic diagram of the multi-head linear self-attention module's structure. In each linear self-attention module, the query, key, and value features are mapped to 64 channels after being processed by a linear layer, and then the processed matrix of key and value is passed through a fully connected layer, the Projection layer. These two matrices are mapped to 256 in the dimension of time length by using the Projection layer. The output value is then calculated using Eq. (18) below.

$$O_i = softmax\left(\frac{QW_i^Q\left(E_iKW_i^K\right)}{\sqrt{d_k}}\right) * F_iVW_i^V \tag{18}$$

where K, Q, and V represent key, query, and value metrics, respectively; E and F represent the fully connected layers in the Projection layer; W represents the weights that can be trained; d_k is the dimension of the hidden layer of the model; *softmax* represents the normalized exponential function; O_i represents the output of one head in the multi-head linear self-attention module. The reason for scaling is to make the gradient drop more stable during the softmax process and to avoid the stagnation of model parameter updates caused by too small gradients.

Finally, concatenate the calculation results of the eight multi-head linear self-attention modules and map them through a linear layer to obtain the final calculation results, as shown in Eq. (19).

$$O = W^O * \begin{Bmatrix} O_1 \\ O_2 \\ \cdots \\ O_8 \end{Bmatrix} \tag{19}$$

where O represents the final output of the multi-head linear self-attention module.

The schematic diagram of the structure of the Feed-Forward module is shown in Fig. 4(c). It consists of a convolutional layer with a kernel size of 1×1, a ReLU layer (Glorot et al., 2011) and a dropout layer, and another convolutional layer with a kernel size of 1×1. The number of input and output channels in all convolutional layers is 512.

3. Experiments and discussions

In this section, four case studies will be presented to test the effectiveness of the proposed method for the structure response time history forecasting on finite element models or real structures. Therefore, this paper utilizes three refined finite element models with different complexities to verify the efficiency and accuracy of the SeisFormer, including a single-story reinforced concrete structure, a three-story reinforced concrete structure, and an eleven-story reinforced concrete irregular structure. Besides, a full-scale shaking table test model of a two-story low-damage concrete wall building is used to verify the accuracy of the SeisFormer model in the case of extreme data scarcity. Finally, comparative experiments were carried out on several essential parameters of the SeisFormer model and the comparison between the accuracy of SeisFormer and LSTM.

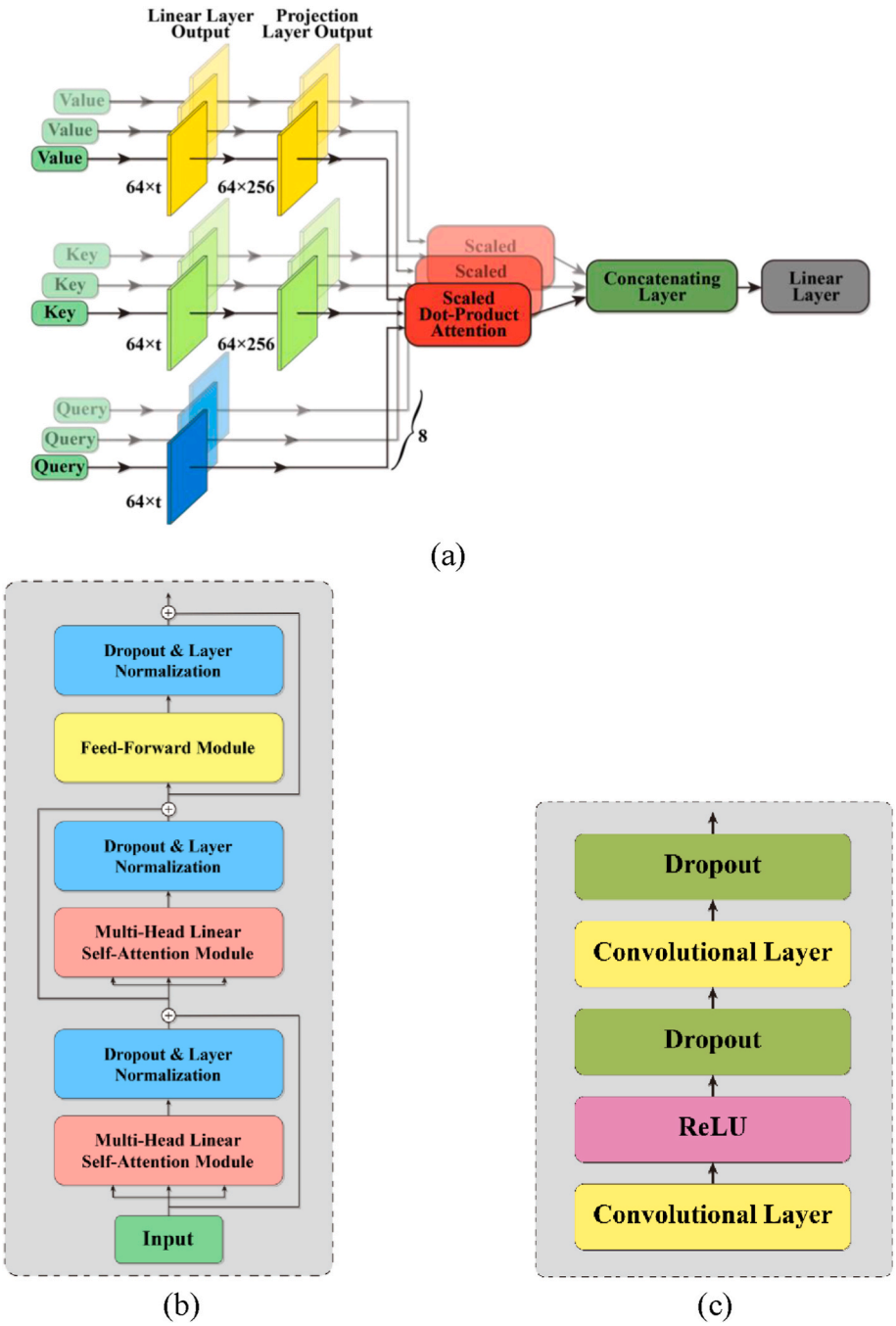

Fig. 4. The detailed structure of the SeisBlock. (a) Shows the structure diagram of the multi-head linear self-attention module; (b) shows the structure diagram of the SeisBlock; (c) shows the structure diagram of the Feed-Forward module, t is the length of the input time steps.

3.1. Dataset generation and training details

In the experimental part of this paper, the finite element model established by ABAQUS is used for elastoplastic seismic time history analysis. The vertical load applied to the structure is the representative value of gravity load. Seismic action is applied to all nodes at the bottom simultaneously. The direction of applying acceleration is the most unfavorable direction for building earthquake resistance.

3.1.1. Dataset generation and training details

Select 200 seismic waves in the Pacific Earthquake Research Center (PEER) ground motion database (Timothy et al., 2013) to perform elastoplastic seismic time history analysis on the three finite element models. The specific information of the selected seismic waves is shown in Appendix A. Since the selected buildings are located in Shanghai, China, according to the local seismic protection intensity, the seismic wave amplitude is adjusted to a random number between 30 and 220 cm/s^2. The sampling interval of seismic waves is 0.02 s. The 200 seismic waves were randomly divided into a training set and a test set according to the ratio of 8:2. Since the structural response is more valuable when the ground motion is relatively large, this paper selects the larger part of the intermediate ground motion data in the original ground motion. Seismic wave values lower than one-tenth of the seismic wave amplitude are removed at the beginning and end of the ground motion because there are a large number of seismic waves with values close to zero at the beginning and end of the original data. In the case of this type of data,

the structure generally does not appear damaged or plastic deformation, so the actual value of this type of data is minimal. During the model training process, 20 seismic waves were randomly selected from the training set as the validation set. The acceleration, velocity, and displacement time histories of all nodes and the acceleration, velocity, and displacement data of ground motion are extracted and divided into a training set and a test set. The SeisFormer model is used to train and test the three types of responses, respectively.

3.1.2. Details of finite element calculations

The finite element calculations in this experiment are performed by ABAQUS software for elastoplastic time-history analysis. In terms of material parameter setting, the materials used in the experiments include concrete materials and steel reinforcement materials. The reinforcement material in the wall or slab element adopts the ideal elastic-plastic model provided by ABAQUS, and the concrete model adopts the elastoplastic damage model provided by ABAQUS. The hysteretic constitutive model of steel and concrete materials adopts the constitutive model stipulated in the Chinese standard "Code for design of concrete structures" (GB 50010-2002). The concrete stress-strain relationship adopts concrete uniaxial stress-strain relationship in Appendix C of the Chinese standard "Code for design of concrete structures" (GB 50010-2002).

In all experiments in this paper, the input load for the finite element model is the ground motion acceleration. The specific method is as follows. First, select the most unfavorable direction of the structure for seismic resistance, and apply the same ground motion acceleration to all nodes connected to the ground in this direction. In addition, the other five degrees of freedom of all nodes connected to the ground are restricted, so their responses are all zero during the entire finite element calculation process.

The calculation method of the finite element model established in this paper is implicit calculation. In the implicit calculation process, each incremental step requires an equilibrium iteration. If the balance condition is not satisfied when calculating a specific incremental step, the incremental step is halved and recalculated until the result converges. After that, the initial incremental step is still used in the subsequent calculation step. If the calculation increment is reduced to a set minimum value, the calculation is aborted. In this paper, the size of the initial incremental step is set to 0.02s, and the preset minimum incremental step is 1×10^{-8} s.

3.1.3. Data preprocessing

In the data preprocessing part, this paper scales all the data during the training of the SeisFormer model. Scale the seismic wave and the time histories of all nodes by the same scale factor, and control the amplitude of all seismic wave time histories to a constant value. However, in the actual prediction, the predicted node time history data is non-destructively restored according to the scale factor of the seismic wave. This paper selects the amplitude of the ground motion data as 3.5. In addition, this paper augments the dataset by overlapping partitioning. Assuming that the number of input structural response time steps is n_i, the number of time steps predicted by the model is n_j, and the number of the total time steps of seismic data is nt. The training set can be divided into $(n_t - n_i - n_j + 1)$ pieces of training data. Each piece of data has ni + nj time steps. In order to show the specific way of overlapping partitioning more clearly, the division method is shown in Fig. 5. Each sequence in Fig. 5 is a piece of training data, and there is only one time step between each sequence. Each sequence represents the input and output of the SeisFormer model in a single prediction. The training set data can be fully utilized through this data set augmentation method, thereby achieving more efficient prediction with fewer data.

3.1.4. Training and evaluation details

The experimental results were evaluated using the Pearson correlation coefficient R and the mean square error (MSE). The closer the Pearson correlation coefficient is to 1, the closer the model predicted results are to the ground truth. The smaller the *MSE*, the closer the predicted result is to the ground truth. The expression for calculating the Pearson correlation coefficient and *MSE* are shown in Eqs. (20) and (21):

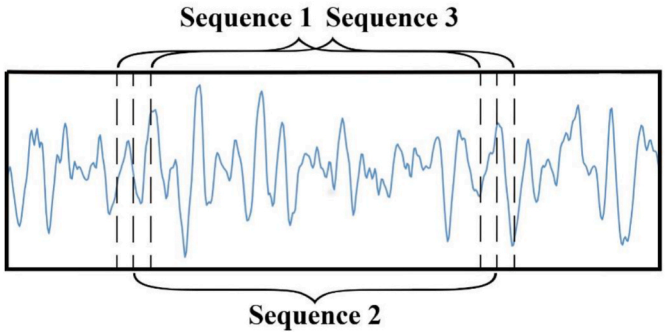

Fig. 5. The schematic diagram of the data augmentation method through overlapping partition.

$$R = \frac{\sum_{i=1}^{N}(X_i - \overline{X})(Y_i - \overline{Y})}{\sqrt{\sum_{i=1}^{N}(X_i - \overline{X})^2}\sqrt{\sum_{i=1}^{N}(Y_i - \overline{Y})^2}} \tag{20}$$

where R is the Pearson correlation coefficient; N represents the total number of time steps; X and Y are the ground truth and predicted result, respectively; X and Y are the mean of the ground truth and predicted result, respectively.

$$MSE = \frac{1}{N}\sum_{i=1}^{N}\sum_{j=1}^{T_i}\left(y_{ij} - \hat{y}_{ij}\right)^2 \tag{21}$$

where *MSE* represents the value of the mean square error; N is the number of seismic waves in the test set; T_i is the total number of time steps for one of the structural response time history; y is the ground truth; $\bar{y}$ is the predicted value of the neural network.

However, due to the different magnitudes of ground motions, the magnitudes of structural responses corresponding to different ground motions may vary significantly. Therefore, directly using *MSE* as an evaluation criterion cannot effectively judge the accuracy of the model prediction. To unify the evaluation criteria, all seismic waves are adjusted to an amplitude of 3.5. The corresponding structural response prediction and actual values use the same adjustment ratio as the seismic waves. In all subsequent experiments in this paper, the adjusted structural response prediction results and ground truth are used to calculate the *MSE*. This operation can eliminate the problem of inconsistent *MSE* standards due to different magnitudes of ground motions.

This paper uses the mean square error function as the loss function in the model training process. The model weights are updated using the Adam (Kingma and Ba, 2014) as the optimizer. The batch size during training is set to 10. Use an exponential decay learning rate and set the decay rate to 0.99 and the learning rate to 0.00001. In this experiment, all models are trained on the entire training set for 100 epochs. The time step length of the structural response used in a single prediction is 150 time steps, and the number of layers of SeisBlock in the SeisFormer model is two layers. The number of channels of the SeiFormer model is set to 512. The time step length of a single prediction is three in Section 3.2 and 3.3, and the time step length of a single prediction in Section 3.4 and 3.5 is 20. The device used in this experiment is Intel(R) Xeon(R) Gold 6248 CPU @ 2.50 GHz, and the GPU is NVIDIA Telsa V100. Finally, the SeisFormer is implemented using the deep learning library PyTorch (Paszke et al., 2019).

3.2. Case study 1: single-story reinforced concrete structure

The structure used in this experiment is the school gate of Tongji University, and the finite element model is built with beam elements and plate-shell elements. The school gate's length, width, and height are 20 m, 6 m, and 6 m. The concrete strength grade is C15 level (the standard value of compressive strength is 15 MPa), and the rebar grades are HPB235 (the standard value of yield strength is 2.35×10^5kPa). The structure on both sides of the school gate is composed of four plate shell members with a thickness of 400 mm. The four columns in the middle of the school gate are frame columns, which are modeled by beam elements. The top plate is a plate shell unit with a thickness of 240 mm. Select the response data of all 132 nodes in the finite element model except the 12 nodes connected to the ground as the training and test data. The photo of the building and the nodes selected in the finite element model is shown in Fig. 6, where the red points in the figure are the selected nodes.

Fig. 7 shows the boxplots of the Pearson correlation coefficient R of the acceleration, velocity, and displacement time history predictions of all 132 nodes of the single-story reinforced concrete structure model on the test set containing 40 seismic waves. The mean, maximum, and minimum R of the acceleration time histories of all nodes in the test set are 0.9805, 0.9991, and 0.6667, respectively. And the corresponding values of velocity and displacement are 0.9746, 0.9995, 0.8386 and 0.9986, 0.9999, 0.9968, respectively. The *MSE* of the acceleration, velocity, and displacement time histories are 0.0544, 0.0170, and 0.0037. It should be noted that the amplitude of the data is adjusted according to the method in Section 3.1.4 during the calculation of *MSE*. The prediction results of the nodes with the highest R and the lowest R are selected for visualization, shown in Fig. 8. Besides, the time required to predict the structural response of one floor under a seismic wave with a duration of 1s is 40.58 ms, which is 193 times faster than the finite element method.

3.3. Case study 2: three-story reinforced concrete structure

The dimensions of the structures in this experiment in the x-direction, y-direction, and z-direction are 23, 19, and 11.05 m, respectively. The concrete strength grade is C25 level (the standard value of compressive strength is 25 MPa), and the rebar grades are HPB300 (the standard value of yield strength is 3×10^5kPa). Beam elements and plate-shell elements are used for finite element modeling, and the structure has a total of 1053 nodes. Select the nodes at the end of the beam or plate shell on the second and third floors, consisting of 109 and 110 nodes. Model training is performed on the selected nodes of the two floors, respectively. The remaining nodes participate in the finite element calculation but are not processed in the forecasting of the SeisFormer. The photo of the building and the nodes selected in the finite element model is shown in Fig. 9, where the red points in the figure are the selected nodes. The nodes on the same floor are divided into the same dataset, and the SeisFormer model is trained by floor. In addition, training and prediction of acceleration, velocity, and displacement time histories are also performed separately.

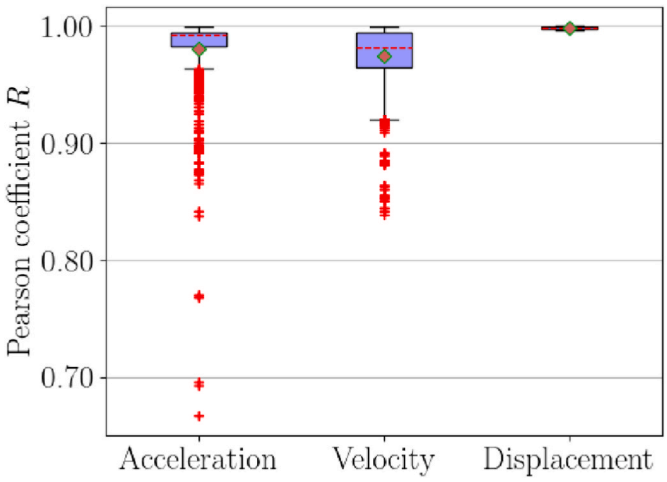

Fig. 7. Boxplots of experimental results for time history prediction of the single-story reinforced concrete structure.

The boxplots of the Pearson correlation coefficient R of acceleration, velocity, and displacement of the selected nodes in the structure on the test set are shown in Fig. 10. The detailed statistics are shown in Tables 1 and 2 according to the evaluation method in Section 3.1.4. Statistical analysis was performed on the test results of all nodes on test set and visualized the best and worst time history data of all selected nodes on the 40 seismic waves, shown in Fig. 11. The mean R of the acceleration time histories of the selected nodes in the test set are 0.9467. And the corresponding values of velocity and displacement are 0.9948 and 0.9991. In addition, the time required to predict the structural response of one floor under a seismic wave with a duration of 1s is 40.49 ms, which is 636 times faster than the finite element method.

3.4. Case study 3: eleven-story reinforced concrete irregular structure

The structure used in this experiment is the library of Tongji University, which is a reinforced concrete irregular structure. The fifth floor and above structure are cantilevered to expand the floor area. The floor height of the building is 3.9 m, and its materials are C20 concrete (the standard value of compressive strength is 20 MPa) and HPB300 steel bars (the standard value of yield strength is 3×10^5kPa). There are 5176 nodes in the finite element model, where eight nodes were selected on floors two to four, and fifty nodes were selected in layers five to eleven for training. The photo of the building and the schematic diagram of node selection in the finite element model is shown in Fig. 12, where the red points in the figure are the selected nodes. In the same way as the previous experiments, the nodes on the same floor are divided into the same dataset, and the SeisFormer model is trained by floor. Besides, training and prediction of acceleration, velocity, and displacement time histories are also performed separately.

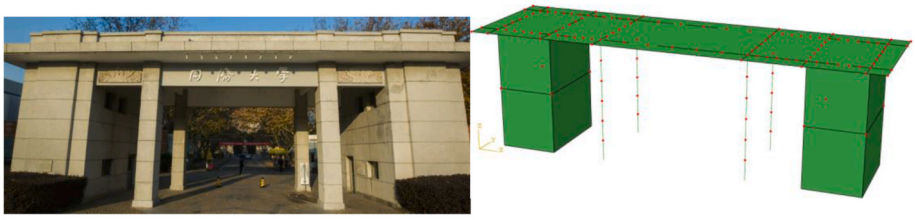

(a) (b)

Fig. 6. The single-story reinforced concrete structure. (a) Shows the photo of the single-story reinforced concrete structure; (b) shows the finite element model of the single-story reinforced concrete structure and selected nodes.

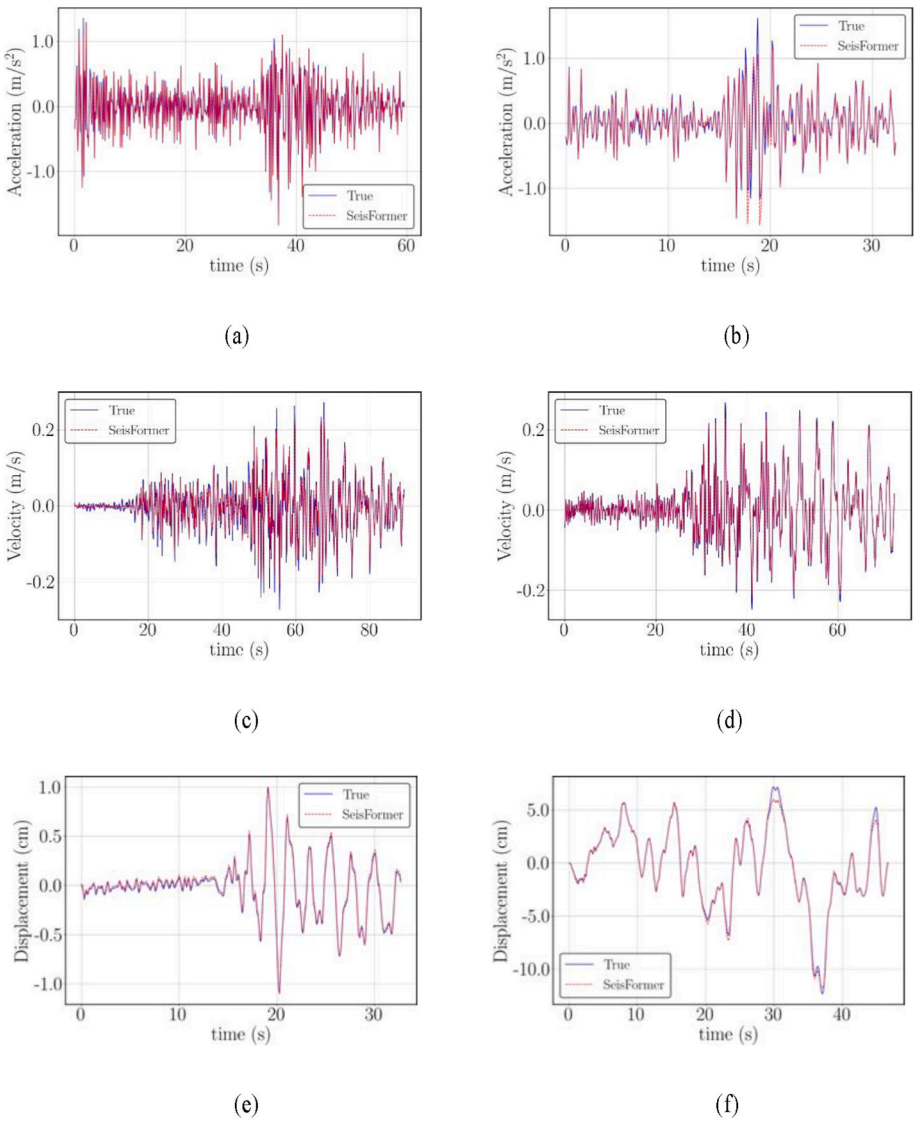

Fig. 8. Visualization of response time history prediction results on the single-story reinforced concrete structure. (a), (c), and (e) show the prediction result of the acceleration, velocity, and displacement time history with the highest R, which are node 40 under the excitation of the RSN18298 seismic wave, node 7 under the excitation of the RSN20842 seismic wave, and node 45 under the excitation of the RSN18179 seismic wave, respectively; (b), (d), and (f) show the prediction result of the acceleration, velocity, and displacement time history with the lowest R, which are node 40 under the excitation of the RSN18179 seismic wave, node 25 under the excitation of the RSN11722 seismic wave, and node 50 under the excitation of the RSN04918 seismic wave, respectively.

Fig. 9. The three-story reinforced concrete structure. (a) Shows the photo of the three-story reinforced concrete structure; (b) shows the finite element model of the three-story reinforced concrete structure and selected nodes.

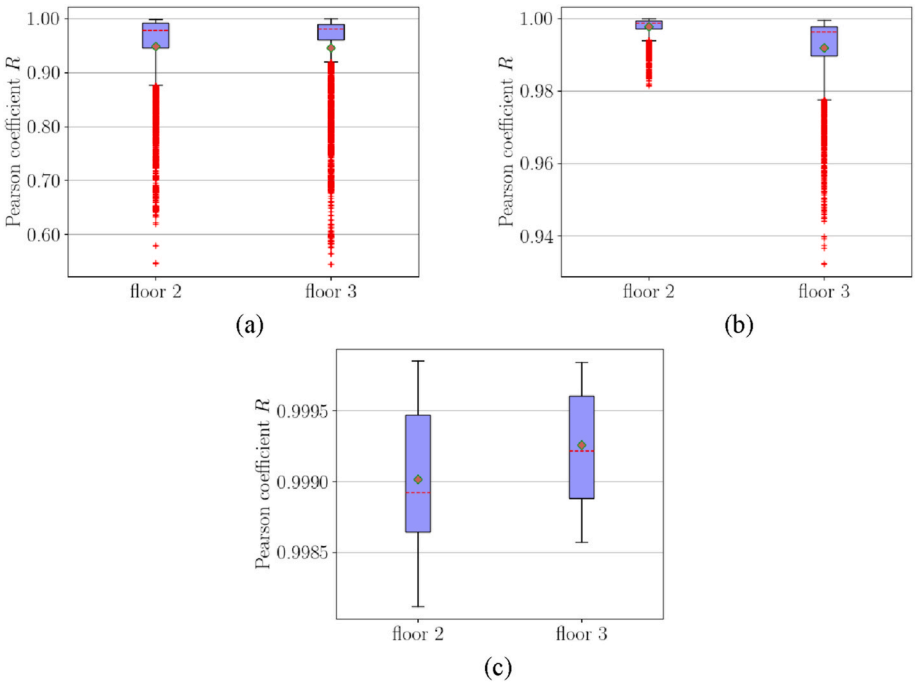

Fig. 10. Boxplots of experimental results for time history prediction of the three-story reinforced concrete structure. (a), (b) and (c) show the experimental results of acceleration time history, velocity time history, and displacement time history prediction, respectively.

Table 1
Statistical results of the R of the case study 2. The left, middle, and right data represent the mean, maximum, and minimum R values, respectively.

Dataset	Acceleration	Velocity	Displacement
floor2	0.9477/0.9988/ 0.5466	0.9977/0.9998/ 0.9814	0.9990/0.9999/ 0.9981
floor3	0.9457/0.9990/ 0.5445	0.9919/0.9994/ 0.9320	0.9993/0.9998/ 0.9986

Table 2
The statistical results of the *MSE* of case study 2.

Dataset	Acceleration	Velocity	Displacement
floor2	0.1536	0.0129	0.0043
floor3	0.4369	0.0398	0.0027

The boxplots of the Pearson correlation coefficient R of acceleration, velocity, and displacement of selected nodes in the structure on the test set are shown in Fig. 13. Moreover, the detailed statistics are shown in Tables 3 and 4 according to the evaluation method in Section 3.1.4. The mean R of the acceleration time histories of the selected nodes in the test set are 0.8970. And the corresponding values of velocity and displacement are 0.9526 and 0.9820. The prediction results of the nodes with the highest R and the lowest R are selected for visualization, shown in Fig. 14. The time required to predict the structural response of one floor under a seismic wave with a duration of 1s is 6.239 ms, which is 109,824 times faster than the finite element method.

3.5. Case study 4: full-scale shaking table test model of a two-story low-damage concrete wall building structure

In this experiment, the measured acceleration and displacement data of the shaking table test model are used to verify the prediction efficiency and accuracy of the SeisFormer when training with an extremely small amount of data in a real building. The real structure is a two-story low-damage concrete wall building. Details and specific parameters of the shaking table test model can be found in the study by Henry et al. (2021). Select five nodes on the second floor of the building to predict the acceleration, and select four nodes to predict the displacement. The photo of the building and the layout of the sensor position is shown in Fig. 15. Five working conditions loaded in the x-direction are selected to train and test the model through k-fold cross-validation. Each training set consists of four ground motions and structural response data, while the test set contains one. The five test conditions are: D1a-25%-x, D1a-25%-x2, D1a-50%-x, D1a-100%-x and D1a-100%-x2 (Henry et al., 2021).

The experiment results show that the five experiments' average, maximum and minimum R of the acceleration time history of the five seismic waves are 0.8460, 0.9568, and 0.7439, respectively. Moreover, the corresponding value of displacement time history is 0.8727, 0.9324, and 0.8320. The boxplot of the experiment results is shown in Fig. 16, while the visualization of the acceleration and displacement prediction result is shown in Fig. 17. The *MSE* of the acceleration and displacement time histories are 2.1755 and 1.6584. It can be seen from the experimental results that although the training data is extremely scarce, the SeisFormer model can still achieve a relatively good training accuracy, which reflects the effect of data augmentation through the autoregressive strategy and the SeisFormer's powerful capabilities in structural response prediction.

3.6. Comparative experiments

This section conducts comparative experiments on several essential parameters in the model and compares the prediction accuracy of the SeisFormer and the LSTM. In order to make the test results more distinguishable, the acceleration data of 50 nodes on the roof of the eleven-story reinforced concrete cylindrical structure are selected as the dataset. First, the time step length of the structure response input by the SeisFormer model is tested, and the test results are shown in Table 5. The experimental results indicate that the model has a strong ability to predict long-term series.

Then, the number of time steps that the SeisFormer outputs in one forward propagation is tested, and the results are shown in Table 6. The

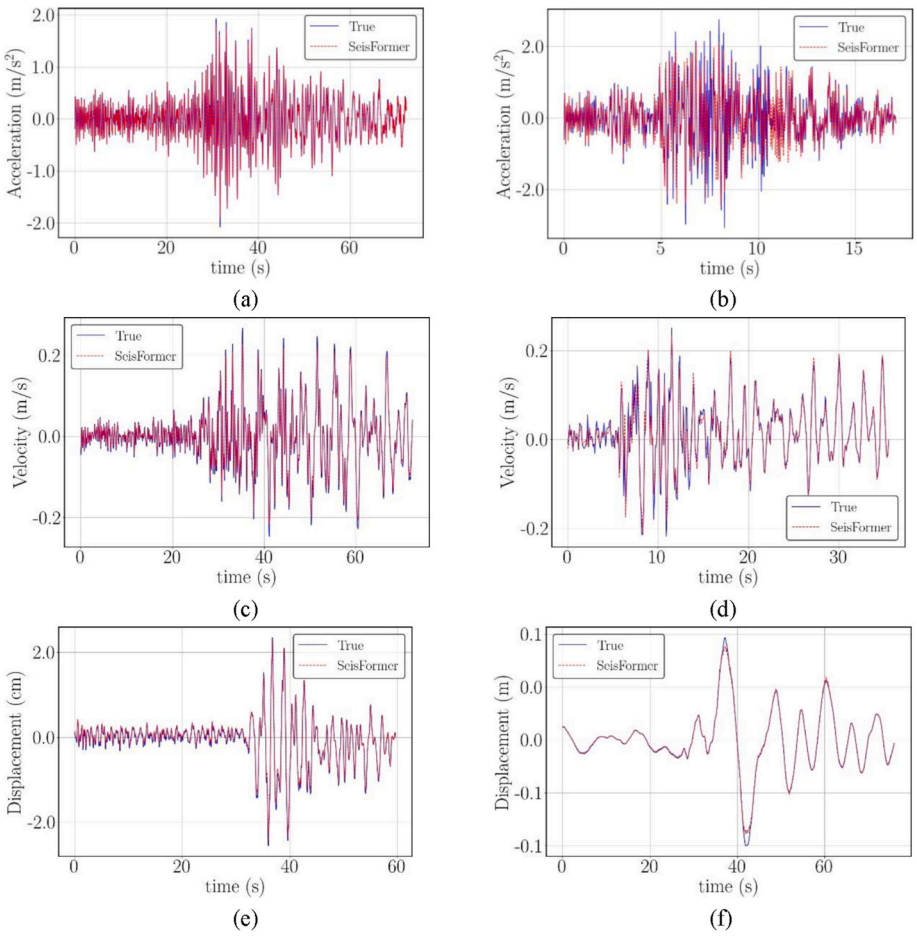

Fig. 11. Visualization of response time history prediction results on the three-story reinforced concrete structure. (a), (c), and (e) show the prediction result of the acceleration, velocity, and displacement time history with the highest R, which are node 11 of the third floor under the excitation of the RSN20842 seismic wave, node 70 of the second floor under the excitation of the RSN20842 seismic wave, and node 21 of the second floor under the excitation of the RSN18298 seismic wave, respectively; (b), (d), and (f) show the prediction result of the acceleration, velocity, and displacement time history with the lowest R, which are node 37 of the third floor under the excitation of the RSN03215 seismic wave, node 26 of the third floor under the excitation of the RSN01977 seismic wave, and node 69 of the second floor under the excitation of the RSN05740 seismic wave, respectively.

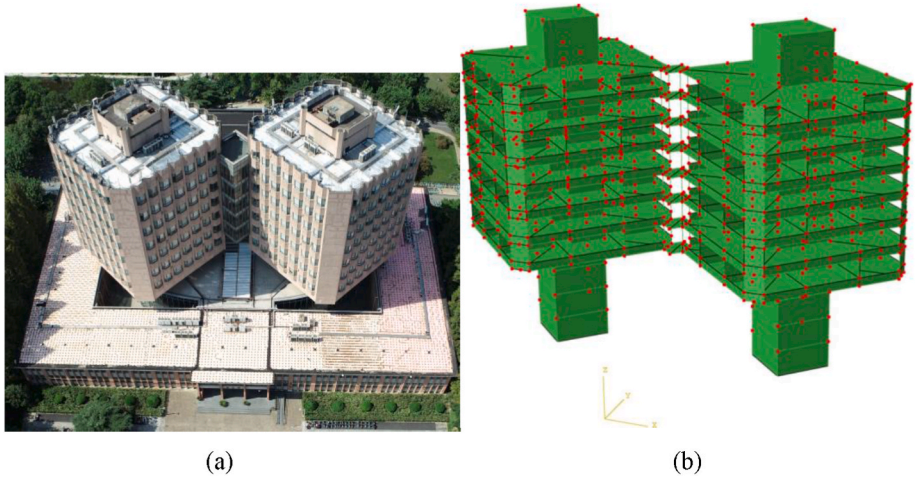

Fig. 12. The eleven-story reinforced concrete irregular structure. (a) Shows the photo of the eleven-story reinforced concrete irregular structure; (b) shows the finite element model of the eleven-story reinforced concrete irregular structure and selected nodes.

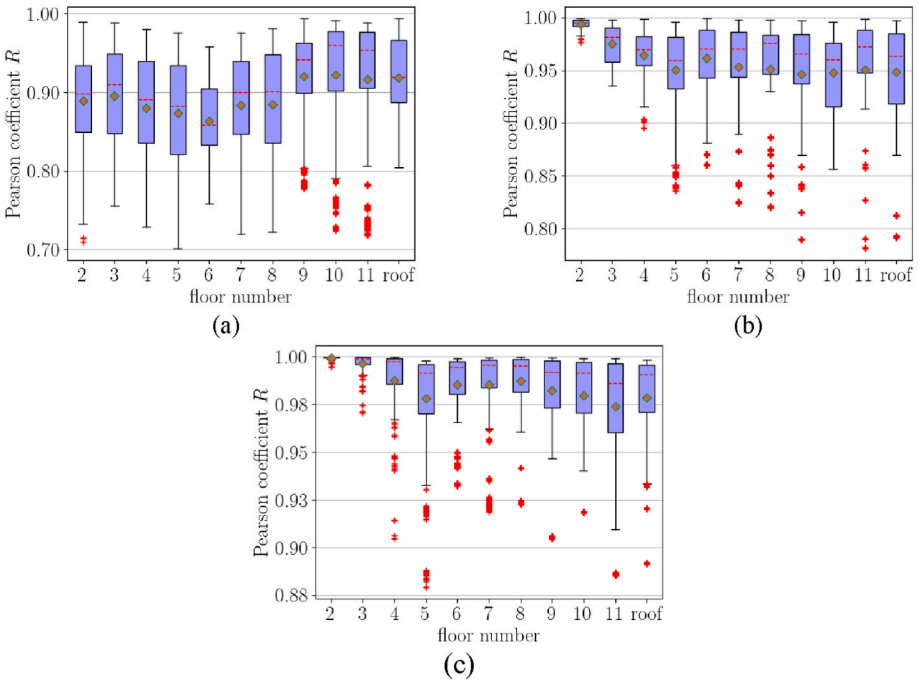

Fig. 13. Boxplots of experimental results for time history prediction of the eleven-story reinforced concrete irregular structure. (a), (b) and (c) show the experimental results of acceleration time history, velocity time history, and displacement time history prediction, respectively.

Table 3
Statistical results of the R of case study 3. The left, middle, and right data represent the mean, maximum, and minimum R values, respectively.

Dataset	Acceleration	Velocity	Displacement
floor2	0.8893/0.9893/ 0.7090	0.9938/0.9995/ 0.9762	0.9994/0.9999/ 0.9945
floor3	0.8950/0.9879/ 0.7551	0.9752/0.9977/ 0.9354	0.9963/0.9998/ 0.9706
floor4	0.8799/0.9799/ 0.7282	0.9643/0.9982/ 0.8947	0.9876/0.9997/ 0.9046
floor5	0.8735/0.9755/ 0.7010	0.9503/0.9955/ 0.8357	0.9780/0.9980/ 0.8791
floor6	0.8629/0.9580/ 0.7585	0.9613/0.9988/ 0.8595	0.9853/0.9990/ 0.9321
floor7	0.8831/0.9752/ 0.7198	0.9529/0.9979/ 0.8234	0.9854/0.9994/ 0.9187
floor8	0.8838/0.9806/ 0.7226	0.9511/0.9979/ 0.8196	0.9871/0.9997/ 0.9224
floor9	0.9204/0.9942/ 0.7761	0.9465/0.9970/ 0.7893	0.9822/0.9996/ 0.9045
floor10	0.9218/0.9913/ 0.7234	0.9479/0.9960/ 0.8564	0.9797/0.9990/ 0.9181
floor11	0.9163/0.9882/ 0.7180	0.9503/0.9986/ 0.7808	0.9740/0.9992/ 0.8850
roof	0.9181/0.9939/ 0.8040	0.9444/0.9968/ 0.7893	0.9783/0.9982/ 0.8914

results show that the model is more accurate for long-term trend prediction. Finally, a comparative study on the accuracy of the Seisformer model and the LSTM model for structural time history prediction under seismic action is performed, and the results are shown in Table 7 and Fig. 18. It can be seen that the SeisFormer model significantly outperforms the LSTM model.

3.7. Discussions

The method proposed in this paper can effectively realize the high-precision real-time response prediction of multiple nodes in the building structure under earthquake action. The proposed model's effectiveness, accuracy, and computational efficiency have been fully

Table 4
The statistical results of the *MSE* of case study 3.

Dataset	Acceleration	Velocity	Displacement
Floor2	0.1365	0.0098	0.0018
Floor3	0.1946	0.0458	0.0093
Floor4	0.3686	0.0768	0.0345
Floor5	0.6283	0.1525	0.0825
Floor6	0.6388	0.1588	0.0679
Floor7	0.6514	0.2602	0.0768
Floor8	0.6183	0.3715	0.1044
Floor9	0.4125	0.5183	0.1693
Floor10	0.4980	0.6674	0.1835
Floor11	0.7997	0.8084	0.1880
Roof	0.9007	1.0813	0.1971

verified through several experiments in multiple buildings. However, the method proposed in this paper has certain limitations. First of all, it can be seen from the experimental results of Case 3 that the SeisFormer proposed in this paper has a worse effect on predicting the structural response of higher floors than lower floors. Therefore, the application in super high-rise buildings may be limited. In addition, the method proposed in this paper is only implemented through a data-driven approach without embedding the physical and structural information of the building structure. Finally, existing real-time seismic response prediction methods have the problem of being difficult to migrate between multiple buildings. In future research, the physical and structural information of building structures can be embedded in data-driven models to achieve higher accuracy and more generalizable structural response prediction.

4. Conclusion

This paper proposes a real-time refined and high-precision response prediction method for structures under seismic action. The proposed SeisFormer model can realize real-time structural response time history prediction for a large number of nodes in the structure. Using the autoregressive mechanism reduces the demand for data volume, and the model's robustness and generalization are significantly improved. By

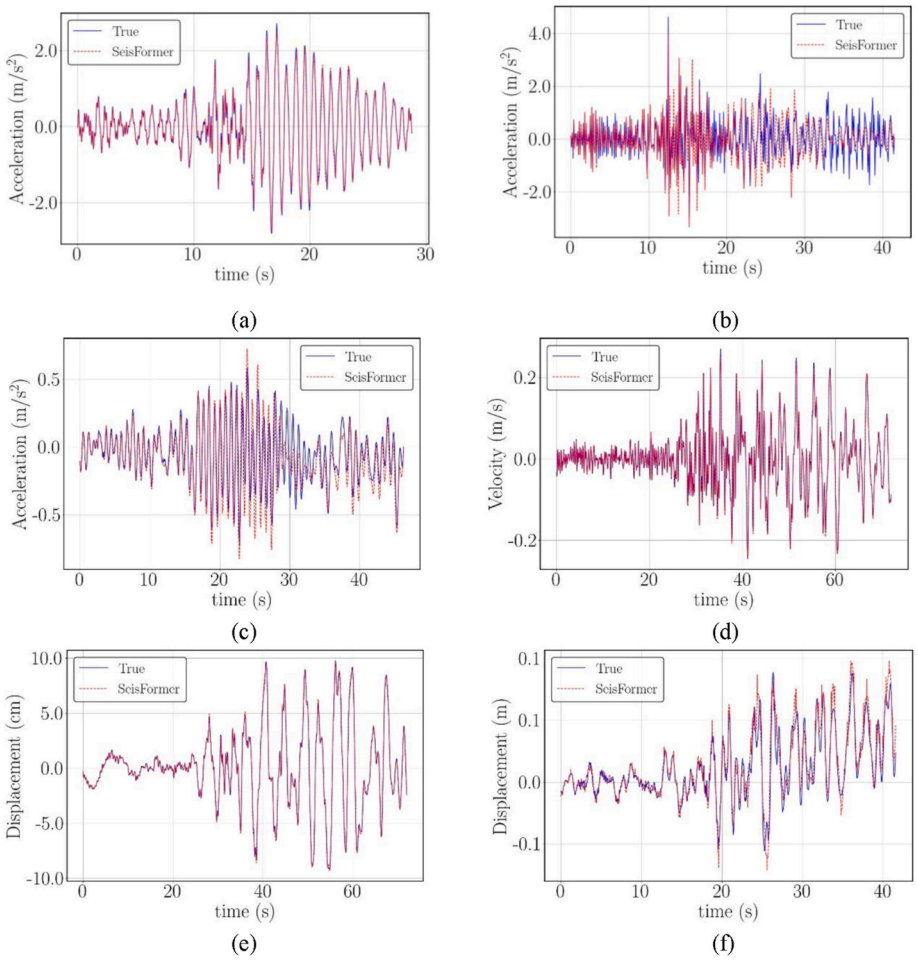

Fig. 14. Visualization of response time history prediction results on the eleven-story reinforced concrete irregular structure. (a), (c), and (e) show the prediction result of the acceleration, velocity, and displacement time history with the highest R, which are node 27 of the ninth floor under the excitation of the RSN12926 seismic wave, node 1 of the second floor under the excitation of the RSN20842 seismic wave, and node 4 of the second floor under the excitation of the RSN20842 seismic wave, respectively; (b), (d), and (f) show the prediction result of the acceleration, velocity, and displacement time history with the lowest R, which are node 37 of the fifth floor under the excitation of the RSN19952 seismic wave, node 44 of the eleventh floor under the excitation of the RSN04918 seismic wave, and node 28 of the fifth floor under the excitation of the RSN20450 seismic wave, respectively.

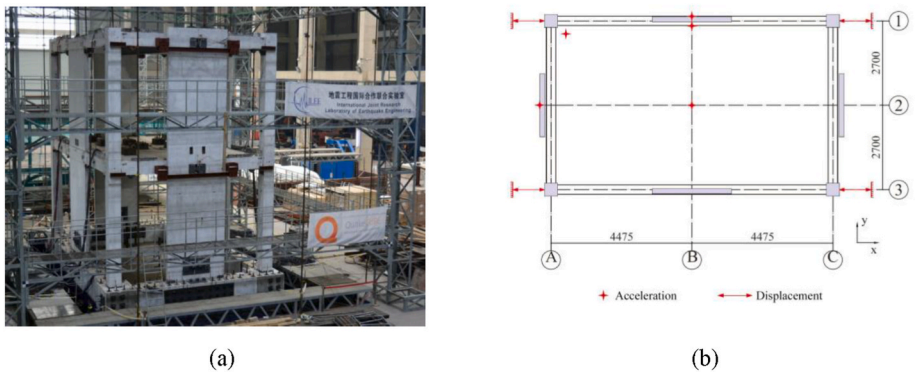

Fig. 15. The full-scale shaking table test model of a two-story low-damage concrete wall building structure. (a) Shows the photo of the test building; (b) shows the selected sensors (Henry et al., 2021).

establishing SeisBlock, the structural response time histories of multiple time steps can be predicted simultaneously in one prediction, which significantly improves the prediction efficiency of the model and reduces the cumulative error. Four case studies, including a single-story reinforced concrete structure, a three-story reinforced concrete structure, an eleven-story reinforced concrete irregular structure, and a two-story shaking table test model, are presented to verify the proposed method's feasibility, efficiency, and accuracy. Finally, through two ablation studies and one comparative experiment, the hyperparameters in the SeisFormer are investigated, and the comparison between the SeisFormer and the LSTM model is presented. From the obtained results, the following conclusions can be drawn:

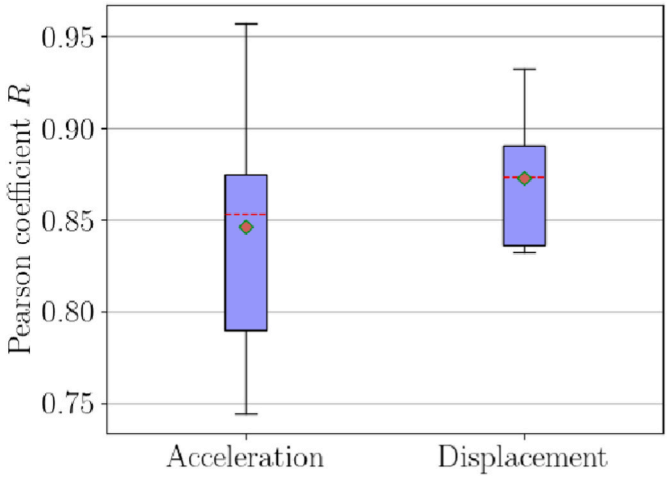

Fig. 16. Boxplot of experimental results for time history prediction of the full-scale shaking table test model of a two-story low-damage concrete wall building structure.

(1) The method proposed in this paper can realize the real-time prediction of the structural response under seismic action, and its prediction speed is 193–109824 times faster than that of the finite element method. The average Pearson correlation coefficient R of the predicted acceleration time histories can reach 0.9889, 0.9467 and 0.8941 on the single-story reinforced concrete structure, the three-story reinforced concrete structure, and the eleven-story reinforced concrete irregular structure. And the corresponding values of velocity and displacement are 0.9916, 0.9948, 0.9845 and 0.9991, 0.9991, 0.9978. In addition, the amplitude-adjusted structural responses were also evaluated using *MSE*. The accuracy and computational efficiency of the model are verified.

(2) The experimental results of the proposed method on the full-scale shaking table test model show that the combining the autoregressive strategy used in this paper, the SeisFormer can achieve high-precision prediction with extremely limited data. Therefore, the common problem of lack of data in engineering can be effectively solved.

(3) The SeisFormer model can predict the response time histories of a large number of nodes in the structure in a single prediction, so it is possible to achieve refined response time history prediction for all building structures. Thus, it can be used for refined structural damage assessment and other applications in subsequent processing.

(4) The time step length of the structure response input by the SeisFormer model and the time step length of a single prediction of the model was tested by ablation experiments. The experimental results show that the SeisFormer model effectively extracts features from the previous structural response information. In addition, the simultaneous prediction of multiple time steps in the model has better accuracy and efficiency.

Table 7
Comparative experiment of the model.

Model	Average R	Maximum R	Minimum R	*MSE*
LSTM	0.6470	0.8936	0.3857	2.8303
SeisFormer	0.9181	0.9939	0.8040	0.9007

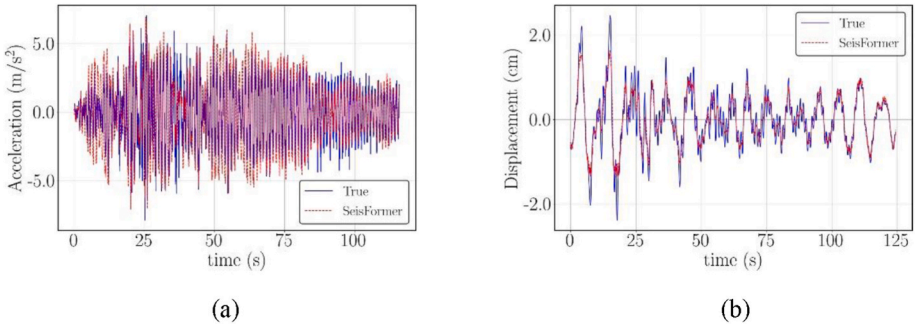

Fig. 17. Visualization of response time history prediction results on the full-scale shaking table test model of a two-story low-damage concrete wall building structure. (a) Shows the prediction result of the acceleration time history, which is node 4 under the excitation of the D1a-50%-x seismic wave; (b) shows the prediction result of the displacement time history, which is node 0 under the excitation of the D1a-50%-x seismic wave.

Table 5
Comparative experiment of the time step length of the structure response input by the SeisFormer model.

Input length	50	100	150	200	250	300	350	400	450	500
Average R	0.8583	0.8982	0.9181	0.9102	0.9040	0.9295	0.9082	0.9062	0.9178	0.9321
Maximum R	0.9730	0.9748	0.9939	0.9910	0.9815	0.9920	0.9845	0.9886	0.9921	0.9944
Minimum R	0.7058	0.7966	0.8040	0.7176	0.8033	0.8171	0.8087	0.7054	0.7074	0.8008
MSE	1.5366	1.1506	0.9007	0.9947	1.0422	0.7929	1.1359	1.1339	1.0642	0.9135

Table 6
Comparative experiment of the time step length of a single prediction.

Input lenth	1	2	3	4	5	10	15	20	25	30	40	50
Average R	0.8209	0.8957	0.9053	0.9129	0.9069	0.9138	0.9055	0.9181	0.9136	0.9005	0.9258	0.9246
Maximum R	0.9577	0.9851	0.9789	0.9908	0.9807	0.9922	0.9837	0.9939	0.9892	0.9901	0.9913	0.9959
Minimum R	0.7121	0.6881	0.8285	0.7170	0.8170	0.7950	0.7132	0.8040	0.8267	0.6933	0.8272	0.7520
MSE	2.1220	1.1517	1.0809	0.9904	1.0287	0.9339	1.0322	0.9007	0.9260	1.2307	0.8154	0.8163

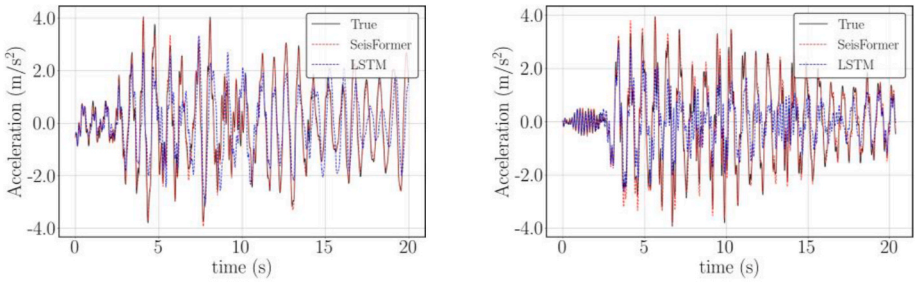

Fig. 18. Visualization of the prediction results of the SeisFormer and the LSTM on the roof of the eleven-story reinforced concrete cylindrical structure. (a) Shows the prediction result of the acceleration time history, which is node 15 under the excitation of the RSN04528 seismic wave; (b) shows the prediction result of the acceleration time history, which is node 27 under the excitation of the RSN05668 seismic wave.

(5) The comparative experiment results of the proposed SeisFormer model and the LSTM model show that the prediction accuracy of the proposed model is significantly better than that of the traditional LSTM model.

CRediT authorship contribution statement

Shiqiao Meng: Conceptualization, Data curation, Investigation, Methodology, Software, Writing – original draft. **Ying Zhou:** Conceptualization, Supervision, Funding acquisition, Writing – review & editing. **Zhiyuan Gao:** Data curation, Software.

Declaration of competing interest

The authors declare that they have no known competing financial interests or personal relationships that could have appeared to influence the work reported in this paper.

Data availability

Data will be made available on request.

Acknowledgments

The authors gratefully acknowledge the financial support from the Distinguished Young Scientist Fund of National Natural Science Foundation of China (Grant No. 52025083), Shanghai "Science and Technology Innovation Action Plan" Social Development Science and Technology Research Project (Grant No. 22dz1201400), National Natural Science Foundation of China (Grant No. U2139209), and the Shanghai Urban Digital Transformation Special Fund (Grant No. 202201033).

Appendix A. The 200 selected ground motion records used in experiments

Table A1
Seismic waves in the PEER ground motion database.

RSN numbers of seismic waves					
Training set					
RSN01325	RSN01593	RSN01630	RSN01780	RSN01805	RSN01833
RSN02039	RSN02115	RSN02165	RSN02173	RSN02246	RSN02331
RSN02339	RSN02342	RSN02393	RSN02418	RSN02434	RSN02483
RSN02491	RSN02550	RSN02603	RSN02672	RSN02715	RSN02722
RSN02776	RSN02803	RSN02832	RSN02846	RSN02925	RSN02948
RSN02982	RSN02988	RSN03001	RSN03055	RSN03065	RSN03151
RSN03202	RSN03235	RSN03292	RSN03318	RSN03376	RSN03410
RSN03442	RSN03445	RSN03862	RSN03920	RSN04039	RSN04045
RSN04111	RSN04199	RSN04410	RSN04483	RSN04860	RSN04914
RSN04923	RSN05128	RSN05259	RSN05275	RSN05449	RSN05506
RSN05566	RSN05584	RSN05592	RSN05596	RSN05683	RSN05829
RSN06008	RSN06027	RSN06160	RSN06200	RSN06324	RSN06330
RSN06416	RSN06439	RSN06468	RSN06533	RSN06553	RSN06589
RSN06704	RSN06708	RSN06818	RSN06884	RSN06897	RSN06958
RSN06970	RSN08135	RSN08154	RSN08176	RSN08233	RSN08268
RSN08758	RSN08804	RSN08812	RSN08825	RSN08933	RSN09140
RSN09145	RSN09149	RSN09170	RSN09188	RSN09774	RSN09974
RSN09978	RSN10532	RSN10685	RSN11010	RSN11123	RSN11600
RSN11717	RSN11742	RSN11816	RSN11853	RSN11922	RSN12177
RSN12703	RSN12868	RSN12874	RSN14080	RSN14312	RSN15073
RSN18002	RSN18027	RSN18103	RSN18195	RSN18386	RSN18983
RSN19501	RSN19511	RSN19714	RSN19753	RSN20069	RSN20158
RSN20409	RSN20687	RSN20751	RSN20799	RSN20834	RSN20841
RSN20865	RSN20866				
Validation set					
RSN01812	RSN02238	RSN02396	RSN02587	RSN02793	RSN02961
RSN03125	RSN03352	RSN03915	RSN04363	RSN04991	RSN05529
RSN05780	RSN06252	RSN06532	RSN06766	RSN08124	RSN08275
RSN08967	RSN09305				

(*continued on next page*)

Table A1 (*continued*)

RSN numbers of seismic waves					
Test set					
RSN01404	RSN01830	RSN01977	RSN02025	RSN02524	RSN02529
RSN02767	RSN02790	RSN03215	RSN03863	RSN04100	RSN04107
RSN04528	RSN04918	RSN05137	RSN05243	RSN05355	RSN05595
RSN05668	RSN05740	RSN05810	RSN05865	RSN06454	RSN06854
RSN06927	RSN08199	RSN08214	RSN10720	RSN11635	RSN11722
RSN12926	RSN18179	RSN18298	RSN19523	RSN19612	RSN19952
	RSN20450	RSN20744	RSN20745	RSN20842	

References

Adeli, H., Jiang, X., 2006. Dynamic fuzzy wavelet neural network model for structural system identification. J. Struct. Eng. 132, 102–111.

Asgarieh, E., Moaveni, B., Stavridis, A., 2014. Nonlinear finite element model updating of an infilled frame based on identified time-varying modal parameters during an earthquake. J. Sound Vib. 333, 6057–6073.

Azimi, M., Pekcan, G., 2020. Structural health monitoring using extremely compressed data through deep learning. Comput. Aided Civil Infrastruct. Eng. 35, 597–614.

Bretas, E.M., Lemos, J.V., Lourenço, P.B., 2016. Seismic analysis of masonry gravity dams using the discrete element method: implementation and application. J. Earthq. Eng. 20, 157–184.

Gao, J., Zhang, C., 2020. Structural seismic response prediction based on long short-term memory network. Earthq. Resist. Eng. Retrofit. 42, 130–136.

Glorot, X., Bordes, A., Bengio, Y., 2011. Deep sparse rectifier neural networks. In: Proceedings of the Fourteenth International Conference on Artificial Intelligence and Statistics, JMLR Workshop and Conference Proceedings, pp. 315–323.

Henry, R.S., Zhou, Y., Lu, Y., Rodgers, G.W., Gu, A., Elwood, K.J., Yang, T.Y., 2021. Shake-table test of a two-storey low-damage concrete wall building. Earthq. Eng. Struct. Dynam. 50, 3160–3183.

Hou, S., Liu, Y., 2022. Early warning of tunnel collapse based on adam-optimised long short-term memory network and tbm operation parameters. Eng. Appl. Artif. Intell. 112, 104842.

Jiang, X., Adeli, H., 2005. Dynamic wavelet neural network for nonlinear identification of highrise buildings. Comput. Aided Civ. Infrastruct. Eng. 20, 316–330.

Ketkar, N., Santana, E., 2017. Deep Learning with Python, vol. 1. Springer.

Kingma, D.P., Ba, J., 2014. Adam: a method for stochastic optimization. preprint arXiv: 1412.6980 arXiv.

Li, T., Pan, Y., Tong, K., Ventura, C.E., de Silva, C.W., 2021a. Attention-based sequence-to-sequence learning for online structural response forecasting under seismic excitation. IEEE Trans. Syst., Man, Cybern.: Syst.

Li, T., Pan, Y., Tong, K., Ventura, C.E., de Silva, C.W., 2021b. A multi-scale attention neural network for sensor location selection and nonlinear structural seismic response prediction. Comput. Struct. 248, 106507.

Liang, X., 2019. Image-based post-disaster inspection of reinforced concrete bridge systems using deep learning with bayesian optimization. Comput. Aided Civ. Infrastruct. Eng. 34, 415–430.

Mohan, R., Prabha, C., 2011. Dynamic analysis of rcc buildings with shear wall. Int. J. Earth Sci. Eng. 4, 659–662.

Morfidis, K., Kostinakis, K., 2018. Approaches to the rapid seismic damage prediction of r/c buildings using artificial neural networks. Eng. Struct. 165, 120–141.

Naser, M., 2019. Ai-based cognitive framework for evaluating response of concrete structures in extreme conditions. Eng. Appl. Artif. Intell. 81, 437–449.

Nie, Y., Sheikh, A., Griffith, M., Visintin, P., 2022. A damage-plasticity based interface model for simulating in-plane/out-of-plane response of masonry structural panels. Comput. Struct. 260, 106721.

Nikolopoulos, S., Kalogeris, I., Papadopoulos, V., 2022. Non-intrusive surrogate modeling for parametrized time-dependent partial differential equations using convolutional autoencoders. Eng. Appl. Artif. Intell. 109, 104652.

Oh, B.K., Glisic, B., Park, S.W., Park, H.S., 2020. Neural network-based seismic response prediction model for building structures using artificial earthquakes. J. Sound Vib. 468, 115109.

Paszke, A., Gross, S., Massa, F., Lerer, A., Bradbury, J., Chanan, G., Killeen, T., Lin, Z., Gimelshein, N., Antiga, L., et al., 2019. Pytorch: an imperative style, high-performance deep learning library. Adv. Neural Inf. Process. Syst. 32.

Peng, H., Yan, J., Yu, Y., Luo, Y., 2021. Time series estimation based on deep learning for structural dynamic nonlinear prediction. In: Structures. Elsevier, pp. 1016–1031.

Perez-Ramirez, C.A., Amezquita-Sanchez, J.P., Valtierra-Rodriguez, M., Adeli, H., Dominguez-Gonzalez, A., Romero-Troncoso, R.J., 2019. Recurrent neural network model with bayesian training and mutual information for response prediction of large buildings. Eng. Struct. 178, 603–615.

Rainieri, C., Fabbrocino, G., 2014. Operational Modal Analysis of Civil Engineering Structures, vol. 142. Springer, New York, p. 143.

Srivastava, N., Hinton, G., Krizhevsky, A., Sutskever, I., Salakhutdinov, R., 2014. Dropout: a simple way to prevent neural networks from overfitting. J. Mach. Learn. Res. 15, 1929–1958.

Timothy, A., Robert, D., Jonathan, S., Emel, S., Walter, S., Brian, C., Katie, W., Robert, G., Albert, K., David, B., Tadahiro, K., Jennifer, D., 2013. Pacific Earthquake Engineering Research Center Nga-West2 Database. https://ngawest2.berkeley.edu/.

Vaswani, A., Shazeer, N., Parmar, N., Uszkoreit, J., Jones, L., Gomez, A.N., Kaiser, L.-., Polosukhin, I., 2017. Attention is all you need. Adv. Neural Inf. Process. Syst. 30.

Wang, N., Adeli, H., 2015. Self-constructing wavelet neural network algorithm for nonlinear control of large structures. Eng. Appl. Artif. Intell. 41, 249–258.

Wilkinson, S., Hiley, R., 2006. A non-linear response history model for the seismic analysis of high-rise framed buildings. Comput. Struct. 84, 318–329.

Wu, R.T., Jahanshahi, M.R., 2019. Deep convolutional neural network for structural dynamic response estimation and system identification. J. Eng. Mech. 145, 04018125.

Xu, Z., Chen, J., Shen, J., Xiang, M., 2022. Recursive long short-term memory network for predicting nonlinear structural seismic response. Eng. Struct. 250, 113406.

Yu, Y., Yao, H., Liu, Y., 2020. Structural dynamics simulation using a novel physics-guided machine learning method. Eng. Appl. Artif. Intell. 96, 103947.

Zhang, R., Chen, Z., Chen, S., Zheng, J., Büyüköztürk, O., Sun, H., 2019. Deep long short-term memory networks for nonlinear structural seismic response prediction. Comput. Struct. 220, 55–68.

Zhang, R., Liu, Y., Sun, H., 2020a. Physics-guided convolutional neural network (phycnn) for data-driven seismic response modeling. Eng. Struct. 215, 110704.

Zhang, R., Liu, Y., Sun, H., 2020b. Physics-informed multi-lstm networks for metamodeling of nonlinear structures. Comput. Methods Appl. Mech. Eng. 369, 113226.

Zhou, Y., Lu, Z., Dai, K., Jiang, J., Shan, J., 2017. Seismic Design of Building Structures. China Architecture & Building Press.